# Properties of AuIn<sub>2</sub> Resistors for Josephson Integrated Circuits

The influences of film thickness and composition on the resistivity and microstructure of  $AuIn_2$  films, which are used as resistors in Josephson integrated circuits, have been investigated. The films were prepared by evaporating Au and In layers onto SiO-coated Si wafers held at 348 K. The resistivity at 4.2 K was found to be  $\approx 5 \mu\Omega$ -cm for 40-nm-thick films and to vary as  $\approx d^{-0.76}$  over the thickness range 30-250 nm. Corresponding sheet resistances ranged from 0.05 to  $2 \Omega/\Box$ . Resistivity changes were also observed as the composition was altered. A decrease of  $\approx 10\%$  in the In/Au thickness ratio from that of  $AuIn_2$  produced an increase of  $\approx 50\%$  in resistivity. A similar increase in In/Au ratio produced  $\leq 10\%$  decrease in resistivity. Electron microscopy analysis revealed that the grain size of  $AuIn_2$  films increases with film thickness, and is approximately two times smaller for the low In/Au ratio films than for those of nominal or larger In/Au ratios. The factors governing the resistivity of  $AuIn_2$  films were analyzed using the Fuchs surface scattering and Mayadas-Shatzkes (M-S) grain boundary scattering theories. It was found that the M-S theory can be used to explain the resistivity data for a range of choices of r and p, the grain-boundary-reflection and surface-reflection coefficients, respectively. Reasonable agreement was obtained for parameter values between r = 0.31, p = 0,  $pl = 3 \times 10^{-11} \Omega$ -cm<sup>2</sup> and r = 0.74, p = 1,  $pl = 0.8 \times 10^{-11} \Omega$ -cm<sup>2</sup>. The available evidence is interpreted as favoring grain boundary scattering as the dominant scattering mechanism.

## Introduction

Thin film resistors are needed for Josephson integrated circuits for use as load resistors [1] and for damping resonances [2]. It has been shown that AuIn, films can be used to form stable resistors that are compatible with a superconducting Pb-In-Au alloy interconnection metallurgy [3]. Such resistors have been used successfully in a variety of experimental logic and memory circuits [4]. In the fabrication of such circuits, it is desirable to have good process control for close resistor tolerances to be maintained. In addition, future devices and circuits made with smaller dimensions will probably require higher resistance values. To maintain high device packaging densities it would be desirable to achieve this increase in resistance by using a resistor film with a higher sheet resistance. Thus, it is of interest to understand the range of sheet resistances obtainable with AuIn<sub>2</sub> films and the factors that govern the resistivity of such films.

In our work, the range of sheet resistances obtainable with AuIn<sub>2</sub> films of various thicknesses has been investi-

gated and the effect on resistivity of varying the composition about the nominal AuIn<sub>2</sub> composition has been determined. In addition, because previous work indicated that the resistivity of AuIn<sub>2</sub> films may be due to electron scattering from grain boundaries or other defects in the films [3], representative Au-In alloy films were investigated by transmission electron microscopy (TEM) to characterize their microstructures. Results of these experiments have been used to analyze the factors that govern the film resistivities.

#### **Experimental procedure**

Films of  $AuIn_2$  were prepared in vacuum by evaporating a layer of Au followed by a layer of In. For  $AuIn_2$  the thickness ratio is In/Au = 3.074. Substrates were SiO-coated Si wafers that were cleaned *in situ* by using an oxygen discharge and held at 348 K during film deposition. Pressures in the deposition chamber during evaporation were  $\le 6 \times 10^{-5}$  Pa. Evaporation rates of 0.1 and 0.5 nm/s were used for Au and In, respectively. The films were main-

Copyright 1980 by International Business Machines Corporation. Copying is permitted without payment of royalty provided that (1) each reproduction is done without alteration and (2) the *Journal* reference and IBM copyright notice are included on the first page. The title and abstract may be used without further permission in computer-based and other information-service systems. Permission to *republish* other excerpts should be obtained from the Editor.

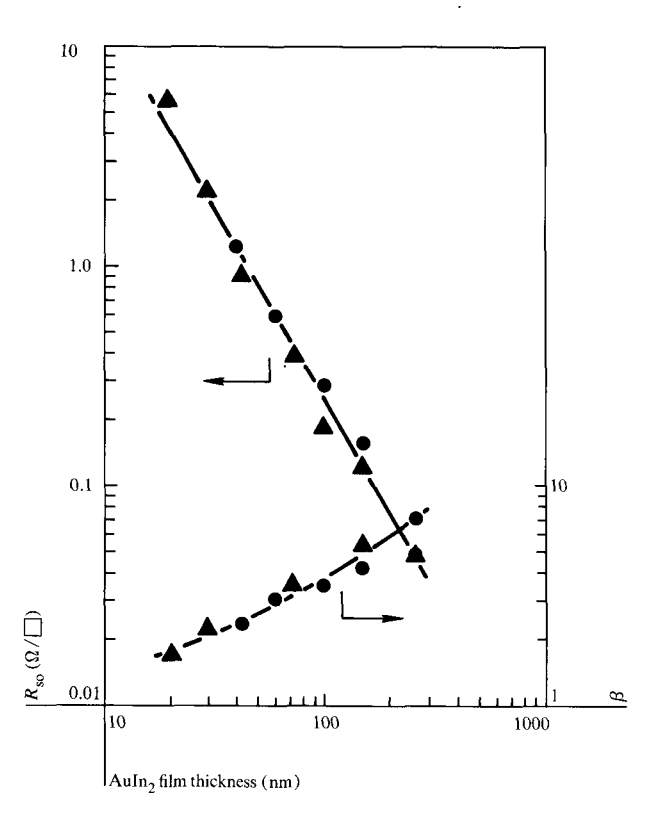


Figure 1 Values of  $R_{s_0}$  and  $\beta$  for AuIn<sub>2</sub> films as a function of film thickness. The  $\bullet$  samples were prepared with companions for TEM analysis.

tained at 348 K for one hour after deposition of the layers to allow the In and Au to interdiffuse to form the  $AuIn_2$  intermetallic compound before removal from the vacuum. Film thicknesses were determined with a quartz crystal deposition monitor calibrated by means of optical interferometry. The  $AuIn_2$  thickness was taken to be the sum of the In and Au thicknesses; this procedure is expected to introduce a thickness error of <1.5% from the values obtained in calculations made with the bulk densities of the film materials.

The AuIn<sub>2</sub> films were patterned using a photoresist stencil lift-off method [5] to form 5-25- $\mu$ m-wide resistors of various lengths with measurement leads. Resistances R were measured using the four-terminal method at ambient temperature ( $\approx$ 297 K), and at 4.2 K by immersing the film in liquid He. Sheet resistances ( $R_s = RW/L$ ) were obtained with lengths L and widths W measured by optical microscopy. Films to be examined by transmission electron microscopy (TEM) were prepared on Si wafers coated with a layer of photoresist followed by a 50-nm-thick layer of evaporated SiO. The amorphous SiO provided the same surface for film nucleation as that used for the resistor samples without interfering with the TEM

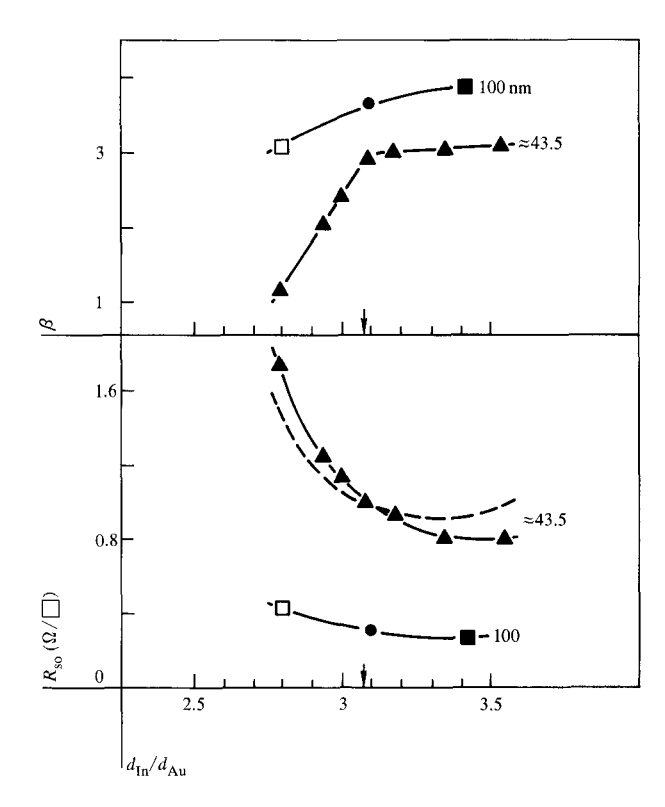


Figure 2 Values of  $R_{\rm so}$  and  $\beta$  for Au-In films with compositions in the vicinity of that for  ${\rm AuIn}_2$  (indicated by arrows). The 100-nm samples were prepared with companions for TEM analysis.

analysis. The photoresist is soluble in acetone and allowed the  $AuIn_2 + SiO$  composite to be transferred to a grid-type film support for TEM analysis.

#### Results

#### • Sheet resistance

The sheet resistances at 4.2 K,  $R_{\rm so}$ , obtained for AuIn<sub>2</sub> films of various thicknesses d, are shown in Fig. 1. The corresponding values of the resistance ratio  $\beta$  $R_{\rm s}(297 \text{ K})/R_{\rm so}$  are also shown. The values of  $R_{\rm so}$  are observed to increase from 0.05 to 5  $\Omega/\Box$  as the thickness is reduced from 250 to 20 nm, following the empirical relation  $R_{\rm so} \propto 844 \ d^{-1.76}$  (d in nm). This thickness dependence is stronger than  $R_{so} \propto d^{-1}$ , indicating that the resistivity  $\rho$ of the AuIn, film material is increasing with decreasing film thickness. In addition, the magnitude of  $R_{so}$  over the range investigated is large compared to the value expected from the bulk resistivity of AuIn<sub>2</sub>. Such high and thickness-dependent resistivities are common for thin films because the film thicknesses, grain sizes, and defectto-defect spacings can be small enough to limit the electron mean free paths in the films. The relative importance of these factors in determining the  $\rho$  of the AuIn, films is

C. J. KIRCHER AND S. K. LAHIRI

discussed later. A useful consequence of this behavior is that the range of  $R_{\rm so}$  values obtainable is considerably extended.

The dependence on composition of  $R_{so}$  for Au-In films has been obtained for compositions near that of AuIn, (In/Au thickness ratio  $d_{\rm In}/d_{\rm Au}=3.074$ ). The data for  $R_{\rm so}$ and for  $\beta$  are shown in Fig. 2 for films 100 nm and ≈43.5 nm thick. The composition variation in the latter case was obtained by using incremental changes in  $d_{\text{in}}$  to allow precise relative compositions to be obtained. (This was done, e.g., by depositing  $d_{Au} = 10.5 \text{ nm}$  and  $d_{In} =$ 30 nm on a group of four samples. A mask was then used to cover one sample and an increment of ≈2.5 nm In was then deposited on the three remaining samples. A second sample was then masked and an additional increment of ≈2.5 nm In was deposited on the two remaining samples. etc.) This procedure resulted in composite film thicknesses of 40-48 nm as  $d_{\rm In}/d_{\rm Au}$  was varied from 2.8-3.6. The contribution of this thickness change to  $R_{so} (d_{ln}/d_{All})$ has been estimated using the data of Fig. 1. The  $R_{so}$  $(d_{\rm in}/d_{\rm Au})$  behavior after adjusting for the effect of these thickness changes is shown by the dashed curve in Fig. 2.

The effect of changing composition on  $R_{\rm so}$  is seen to be much more pronounced for  $d_{\rm In}/d_{\rm Au}$  ratios <3.074 (AuIn<sub>2</sub>). As seen in Fig. 2, an  $R_{so}$  increase of  $\approx 50\%$  is obtained for both AuIn<sub>2</sub> thicknesses as  $d_{\rm In}/d_{\rm Au}$  is reduced by  $\approx 10\%$ from that of AuIn<sub>2</sub> (corrected 43.5-nm curve), while changes in  $R_{so}$  are  $\leq 10\%$  for an  $\approx 10\%$  increase in  $d_{ln}/d_{All}$ . Similar differences in the change in  $\beta$  are observed for films with  $d_{In}/d_{Au}$  above and below the nominal AuIn, composition, particularly for the thinner films. These results indicate significant differences in the distribution of the second-phase material and/or the film microstructure between films with  $d_{In}/d_{Au}$  above and below that of AuIn<sub>2</sub>. The phase diagram for In-Au binary alloys [6a] indicates that AuIn, has a very narrow composition range. Thus, for In concentrations above that of AuIn, a second phase of pure In should develop. For In concentrations below that of AuIn, a second phase of the AuIn intermetallic compound is expected.

One factor contributing to the smaller  $R_{\rm so}$  and  $\beta$  changes for In concentrations above that of  ${\rm AuIn}_2$  can be seen in Fig. 3(a), an SEM of the 100-nm-thick, high-Inconcentration film of Fig. 2. Globules of metal are formed on this film that are not observed for  ${\rm AuIn}_2$  films. The In/Au x-ray fluorescence intensity ratios obtained from such globules using an electron microprobe are  $\approx 3 \times$  higher than those from the surrounding matrix, indicating that the excess amount of In has primarily collected in local regions on the surface. Thus, most of this film is similar in thickness and composition (and hence  $R_{\rm so}$ ) to the  ${\rm AuIn}_2$ 

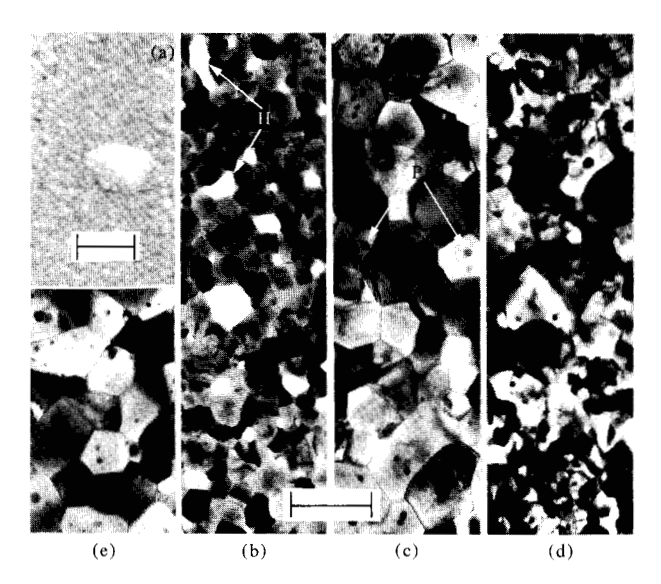


Figure 3 (a) SEM of 100-nm  $AuIn_2$  + In film showing In globule; length mark is  $2 \mu m$ . (b) 20-nm and (c) 100-nm  $AuIn_2$  films showing holes (H) and "particles" (P). TEMs of 100-nm Au-In films with compositions of (d)  $AuIn_2$  + AuIn and (e)  $AuIn_2$  + In; length mark for (b)-(e) is 200 nm.

film. For In concentrations lower than AuIn<sub>2</sub>, such globules are not observed, and thus the AuIn phase appears to be distributed in a more uniform manner in the AuIn<sub>2</sub> matrix.

## Electron microscopy

Resistor samples of several thicknesses of  $\operatorname{AuIn}_2$  (shown as lacktriangle in Fig. 1) and of several compositions (shown as  $\Box$  and  $\blacksquare$  in Fig. 2) were prepared with companion samples for TEM analysis to allow the effect on resistivity of grain size and second-phase particles to be evaluated. Representative electron micrographs from these two sample groups are shown in Figs. 3(b-e). They exhibit several interesting features. Holes are evident in the thinnest (20-nm)  $\operatorname{AuIn}_2$  sample [Fig. 3(b)] and are probably the reason the measured  $R_{so}$  values for samples of this thickness are higher than expected from the  $R_{so} \propto d^{-1.76}$  dependence.

In addition, the grain sizes of the films vary with film thickness [Figs. 3(b, c)] and composition [Figs. 3(d, e)]. Values of the average grain size g (computed using the area method) are plotted in Fig. 4. For AuIn<sub>2</sub> films, g varies linearly with d, increasing from 60 to 220 nm as d is increased from 20 to 260 nm. The value of g for the 100-nm-thick sample with In concentration above that of AuIn<sub>2</sub> ( $\blacksquare$ ) is about equal to that of the AuIn<sub>2</sub> sample. However, g for the 100-nm-thick low-In-concentration sample ( $\square$ ) is only about one-half that of the AuIn<sub>2</sub> sample. Thus, changes in grain size are observed for In-

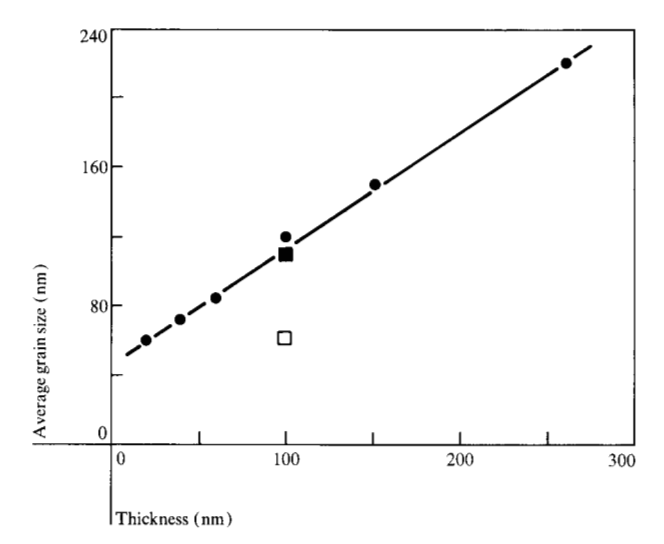


Figure 4 Average grain size of Au-In films as a function of film thickness. Symbols correspond to those in Figs. 1 and 2.

Table 1 Interplanar spacings (nm) calculated from diffraction patterns or obtained from the ASTM file. Spacings set in **bold type** correspond to the highest-intensity diffraction rings; spacings set in *italics* are weak rings of AuIn<sub>2</sub>, as discussed in the text.

AuIn <sub>2</sub>	A T			
+	$AuIn_2$	$AuIn_2 +$	In	$AuIn_2$
AuIn		In		
0.372	0.376	0.372		0.376
0.321	0.322	0.318		
			0.271	
0.263		0.207	<b>0.2</b> .1	
0.203			0.247	
0.227	0.230	0.226		0.230
	0,200	0.220	0.250	0.200
0.210				
0.195	0.195	0.194		0.197
				0.188
	0.107	0.100		0.100
		0 168		
	0.162		0.162	0.163
				0.150
			0.140	0.150
0.17.0	0.175	0.145	0.140	
0.137				
	0.132	0.131	0.150	0.133
			0.124	0.133
0.125 0.124				0.125
				0.113
0 107				0.110
0.107				0.103
	0.372	0.372     0.376       0.321     0.322       0.263     0.227       0.215     0.230       0.195     0.195       0.186     0.189       0.182     0.165       0.161     0.162       0.148     0.149       0.145     0.145       0.137     0.131     0.132       0.124     0.125       0.114     0.109	AuIn         In           0.372         0.376         0.372           0.321         0.322         0.318           0.267         0.263           0.227         0.230         0.226           0.215         0.195         0.194           0.186         0.189         0.186           0.165         0.168         0.161           0.148         0.149         0.147           0.145         0.145         0.143           0.137         0.131         0.132         0.131           0.124         0.125         0.124           0.114         0.114         0.114           0.109         0.109         0.109	AuIn         In           0.372         0.376         0.372           0.321         0.322         0.318           0.267         0.271           0.263         0.247           0.227         0.230         0.226         0.230           0.215         0.195         0.194         0.186         0.182           0.182         0.165         0.168         0.161         0.162         0.161         0.162           0.148         0.149         0.147         0.146         0.145         0.143           0.137         0.134         0.134         0.136         0.136           0.131         0.132         0.131         0.124         0.124           0.114         0.114         0.115         0.109         0.109           0.107         0.108         0.107         0.106

Au films as both thickness and composition are varied. These changes are consistent with the  $R_{\rm so}$  changes observed on companion samples.

Small regions of darker contrast on or within the grains (referred to here as "particles") were observed by TEM in all of the  $AuIn_2$ -containing samples. The volume fraction of these particles was estimated from the bright-field TEM pictures [cf. Figs. 3(b-e)] to be <1%. The volume fraction is approximately independent of film thickness; however, particle size decreases with film thickness.

We do not understand the origin of the particles. They do not appear to be due to a departure from exact stoichiometry (AuIn<sub>2</sub>) since samples intentionally prepared with low- or high-ln content relative to that of AuIn<sub>2</sub> contained particles of similar size and concentration [Figs. 3(d, e)]. The particles do not appear to be an artifact of the preparation procedure since a film of the AuIn intermetallic compound prepared at the same time did not exhibit the particles. Neither have other films prepared using this procedure shown evidence of these particles. Thus, the particles appear to be characteristic of the films containing AuIn<sub>2</sub>.

Transmission electron diffraction patterns were obtained for Au-In films of several compositions by using a relatively large-diameter aperture. The interplanar distances d obtained are summarized in Table 1. For the nominal AuIn, samples, only d values corresponding to AuIn, were observed. (The d values of 0.32, 0.145, and 0.107 nm, corresponding to the {200}, {420}, and {600} planes of AuIn<sub>2</sub>, are not reported on the ASTM data card. Reflections from these planes are expected to be greatly reduced in intensity because the corresponding structure factors are small.) Diffraction patterns from the low- and high-In-content samples show additional diffraction rings due only to AuIn or In phases, respectively, expected from the binary equilibrium phase diagram [6a]. Thus, there is no evidence from the electron diffraction patterns of any unexpected crystalline phase.

A possible explanation for the particles is that they are associated with native oxide formed nonuniformly on the surface of the AuIn<sub>2</sub> films. Such islands of thicker oxide have been reported for Pb [6b] and could produce features (labeled P) observed in Figs. 3(b-e). Although the diffraction patterns showed no evidence of indium oxide, this is not surprising since the volume fraction of the oxide is small.

#### **Analysis**

The values of  $\rho_{f_0}$ , the film electrical resistivity at 4.2 K, have been determined for the AuIn, films from the  $R_{s_0}(d)$ 

data of Fig. 1 and are shown in Fig. 5. The film resistivity is seen to vary strongly with film thickness, increasing from 1.3-7  $\mu\Omega$ -cm as d is decreased from 250-30 nm. These  $\rho_{f_0}$  values are much larger than the value of 0.15  $\mu\Omega$ -cm reported for the resistivity of bulk single crystals of AuIn<sub>2</sub> at 4.2 K,  $\rho_{b_0}$  [7]. We now consider the factors that determine  $\rho_{f_0}$ .

The influence of the particles observed in the AuIn<sub>2</sub> films [Figs. 3(b-c)] on the film resistivity is considered first. The effect would be greatest if the particles were distributed inside the AuIn<sub>2</sub> grains; this situation has been analyzed by Kirkpatrick and Mayadas [8]. Their analysis indicated that 1 vol% of randomly distributed, highly resistive particles would increase  $\rho_{\rm bo}$  by  $\leq 2\%$ , i.e.,  $\Delta \rho < 0.003~\mu\Omega$ -cm. Thus, in our case, the effect of the particles on the film resistivity should be negligible.

#### • Theory

In contrast to the effect of particles, the influence of film surfaces and grain boundaries on  $\rho_{\rm fo}$  can be large. Fuchs and Sondheimer [9] have developed a theory (F-S) for the effect on  $\rho_{\rm f}$  of electron scattering from film surfaces. Their result is

$$\frac{\rho_{t}}{\rho_{1}} = \left[1 - 3 \frac{(1 - p)}{2k} \int_{1}^{\infty} \left(\frac{1}{t^{3}} - \frac{1}{t^{5}}\right) \frac{1 - e^{-kt}}{1 - pe^{-kt}} dt\right]^{-1}$$

$$= \left[1 - A(p, k)\right]^{-1}, \tag{1}$$

where  $k=d/l_i$ ,  $\rho_i$  and  $l_i$  are the intrinsic resistivity and electron mean free path of the material (i.e., in the absence of surfaces and grain boundaries), and p is a phenomenological parameter, the probability that an electron will be specularly reflected from a film surface. Values of p may be selected from 0 to 1 to fit experimental data. A value of p=0 corresponds to diffuse scattering and produces the maximum obtainable value of  $\rho_f$  for a given k. A value of p=1 corresponds to perfect specular (elastic) electron scattering that causes no increase in  $\rho_f$ . Values of p=0-0.5 have given the best fits to single-crystal and large-grain-polycrystalline films [10].

A theory for the effect of grain-boundary scattering on  $\rho_{\text{fo}}$  has been developed by Mayadas and Shatzkes (M-S) [11]. Their result is

$$\frac{\rho_{\rm f}}{\rho_{\rm i}} = [1 - (3\alpha/2) + 3\alpha^2 - 3\alpha^3 \ln(1 + 1/\alpha)]^{-1}$$
$$= [F(\alpha)]^{-1}, \tag{2}$$

where

$$\alpha = (l_i/g)[r/(1-r)] \tag{3}$$

and r is the grain-boundary-reflection coefficient. The more complex case for which grain-boundary and surface

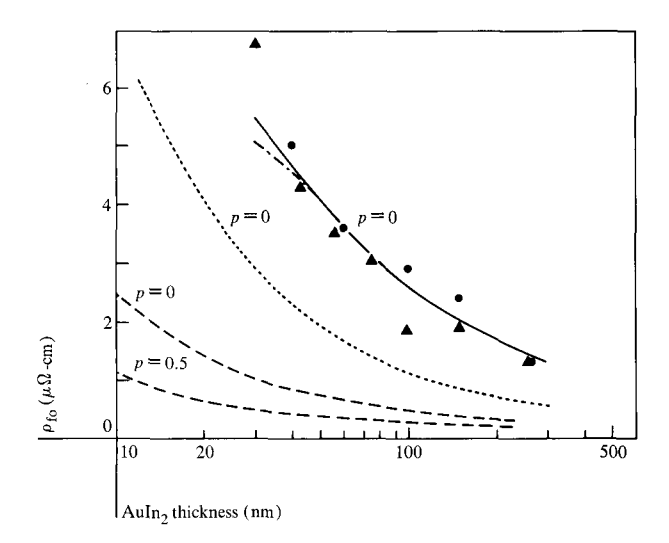


Figure 5 Resistivity of AuIn<sub>2</sub> films at 4.2 K as a function of film thickness. Data points are experimental values. Calculated resistivities obtained using F-S theory are shown as dashed lines  $(\rho l = 0.8 \times 10^{-11} \,\Omega\text{-cm}^2)$  and the dotted line  $(\rho l = 3 \times 10^{-11} \,\Omega\text{-cm}^2, p = 0)$ . Data points obtained using M-S theory are shown as a solid line  $(\rho l = 3 \times 10^{-11} \,\Omega\text{-cm}^2, r = 0.31, p = 0)$  and a dashed-dotted line  $(\rho l = 0.8 \times 10^{-11} \,\Omega\text{-cm}^2, r = 0.71, p = 0)$ .

scattering are both important has also been treated by Mayadas and Shatzkes. Tellier [12] has developed an analytical approximation for the M-S theory that agrees well with M-S over most of the range of interest in this paper  $(k \ge 0.02)$ . His result is

$$\rho_{\rm f}/\rho_{\rm i} = [1 - A(p, k)]^{-1} [F(B)]^{-1}, \tag{4}$$

where

$$B(r, p, k) = \alpha[1 - A(p, k)]$$
 (5)

and A, F, and  $\alpha$  are defined in Eqs. (1)-(3).

## • Estimation of $\rho_i l_i$

The theoretical models express  $\rho_f$  in terms of intrinsic  $\rho_i$  and  $l_i$  values. In practice it is found that the interpretation of  $\rho_{fo}$  data is more sensitive to the  $\rho_i l_i$  product than to the values of  $\rho_i$  and  $l_i$ ;  $\rho l$  is a constant for a given material, given by

$$\rho l = 6\pi^2 h/e^2 S_{\epsilon},\tag{6}$$

where  $S_f$  is the area of the Fermi surface. In the free electron approximation [13]

$$S_{\epsilon} = 4\pi (3\pi^2 n)^{2/3},\tag{7}$$

where n is the carrier concentration. Thus,

$$\rho l = (3/8\pi)^{1/3} (h/e^2) n^{-2/3}. \tag{8}$$

The carrier concentration for AuIn<sub>2</sub> is not known precisely; however, assuming that conduction is due to a

239

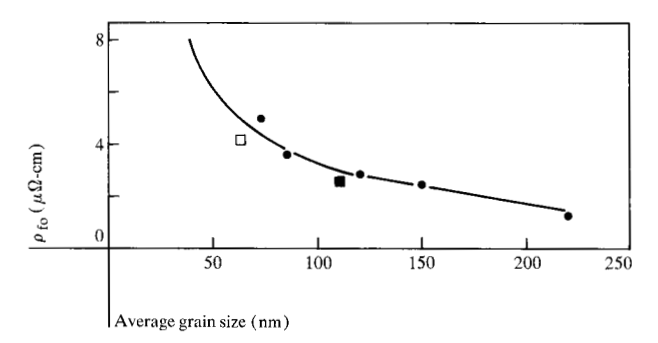


**Figure 6** Resistivity of AuIn<sub>2</sub> films at 4.2 K as a function of average grain size observed by TEM. Data points are experimental values. Calculated resistivities obtained using M-S theory ( $\rho l = 0.8 \times 10^{-11} \ \Omega \text{-cm}^2$ , r = 0.74, p = 1) are shown as a solid line.

**Table 2** Parameter values for which reasonable agreement was obtained between M-S theory and experiment for  $\mathrm{AuIn_2}$  resistivity at 4.2 K. Values of  $l_1 = 0.53$  and 2  $\mu\mathrm{m}$  are most likely for  $\rho l = 0.8 \times 10^{-11} \, \Omega\text{-cm}^2$  and  $3 \times 10^{-11} \, \Omega\text{-cm}$ , respectively, as discussed in the text.

$(10^{-11} \frac{\rho l}{\Omega\text{-cm}^2})$	$l_{\rm i} \ (\mu{ m m})$	p	r
0.8	0.53	1	0.74
0.8	0.53	0	0.71
0.8	0.3	0	0.68
3.0	2	1	0.43
3.0	2	0.5	0.38
3.0	2	0	0.31
3.0	1	0	0.25

single carrier type, a maximum value for n can be estimated [3] from the value of the Hall coefficient  $R_{\rm H}$  reported for bulk single-crystalline  ${\rm AuIn_2}$  [7]. For  $R_{\rm H}=9.3\times10^{-5}~{\rm cm^3/C}$ ,  $n=6.7\times10^{22}/{\rm cm^3}$ , giving an estimated minimum  $\rho l$  of  $0.8\times10^{-11}~\Omega{\rm -cm^2}$ , a value in the range observed for most metals [10, 14]. However, the positive value of  $R_{\rm H}$  indicates that hole conduction dominates and that conduction by both electrons and holes may be important. If so, the actual carrier concentration would be smaller and  $\rho l$  would be correspondingly larger. The range of  $\rho l$  values observed for a wide variety of metals [10, 14] extends to only  $\rho l\approx 3\times10^{-11}~\Omega{\rm -cm^2}$ . Taking this as an upper limit,  $\rho l$  for  ${\rm AuIn_2}$  should be  $0.8{\rm -3}\times10^{-11}~\Omega{\rm -cm^2}$ .

The values of  $\rho_i$  and  $l_i$  can now be estimated. As discussed earlier, the effect of the particles observed in the AuIn, films was judged to be negligible. The vacancy con-

centration should be small due to the high atomic mobility of Au and In in AuIn<sub>2</sub> at 348 K and to the close proximity of surfaces and grain boundaries that serve as vacancy sinks. Other physical defects, such as dislocations or twins, were relatively rare in the films; thus their effect on the intrinsic resistivity is expected to be negligible. We therefore take  $\rho_1 \approx \rho_{\rm bo} = 0.15~\mu\Omega$ -cm. For the  $\rho l$  range estimated above,  $l_1 = l_{\rm bo}$  would then be in the range 0.53-2  $\mu$ m.

# • Interpretation of resistivity data

The interpretation of the  $\rho_{\rm fo}$  (d,g) data using Eqs. (1), (2), and (4) is sensitive to the value of  $\rho l$ . For this reason, and because the  $\rho l$  value is not known very well for AuIn<sub>2</sub>, it is instructive to consider both ends of the  $\rho l$  range previously identified. The case where  $\rho l = 0.8 \times 10^{-11} \,\Omega\text{-cm}^2$  is considered first.

The effect of surface scattering on  $\rho_{\rm fo}$  has been calculated using Eq. (1) for the cases p=0 (maximum surface scattering) and p=0.5 (a commonly observed value) [10]. The results are plotted as the dashed curves in Fig. 5. The calculated  $\rho_{\rm fo}$  values are seen to be much smaller than the experimental ones:  $\approx 5\times$  smaller for the p=0 case. Thus, for  $\rho l=0.8\times 10^{-11}~\Omega\text{-cm}^2$ , surface scattering is not the major factor in determining  $\rho_{\rm fo}$ .

The grain-boundary-scattering theory is now considered for the case p=1, i.e., surface scattering is assumed to be negligible, thereby simplifying the analysis. The  $\rho_{\rm fo}$  (g) data for the samples of Figs. 1 and 4 are plotted in Fig. 6, together with  $\rho_{\rm fo}$  values (solid curve) calculated from Eq. (2). The data can be fitted by using a value of r=0.74. The data points for the 100-nm-thick samples of high ( $\blacksquare$ ) and low ( $\square$ ) In concentration are also included; these also fall near the r=0.74 curve for  $\rho_{\rm fo}$ . Thus, the  $\rho_{\rm fo}$  (g) data can be explained using a hypothesis that scattering from grain boundaries is the dominant electron-scattering mechanism.

The value of r required to fit the data, however, is  $\approx 3 \times$  higher than the values used to fit  $\rho_f$  data on other metal films evaporated in high vacuum [11, 15]. The use of smaller  $l_i$  values (at constant  $\rho_i l_i$ ) has little effect on the r required (Table 2). Combining surface and grain boundary scattering [Eq. (4)] allows r to be reduced only to  $\approx 0.71$ , as shown in Fig. 5. Thus, for  $\rho l = 0.8 \times 10^{-11} \,\Omega$ -cm², the large  $\rho_{fo}$  values and the observed dependence of  $\rho_{fo}$  on d can be explained using the theories only by assuming a larger than typical value of the grain-boundary-reflection coefficient.

The case  $\rho l = 3 \times 10^{-11} \,\Omega$ -cm<sup>2</sup> is now considered. The combined grain-boundary- and surface-scattering case

[Eq. (4)] is used to allow smaller r values to be obtained. Calculated values of  $\rho_{fo}$  for p = 0 and r = 0.31 are shown as the solid curve in Fig. 5. Good agreement is observed between the calculated and measured values. The growing disparity, apparent at  $d \leq 35$  nm, is primarily a consequence of Eq. (4) no longer being a sufficiently good approximation to the full M-S theory. For example, Tellier [12] shows that M-S would give  $\rho_f$  (30 nm)  $\approx 1.2 \times$ higher, in good agreement with the measured values. Thus, the  $\rho_{f_0}$  data can be explained by a combination of surface and grain-boundary scattering, with r values close to the range observed for other films. The shape of  $\rho_{\rm fo}\left(d\right)$ and the value of r needed to obtain agreement with the data are again only weakly dependent upon the choice of l.; however, reasonable agreement can also be obtained for other choices of r and p. Several such sets of parameters are listed in Table 2. Agreement could not be obtained for the pure surface-scattering case (p = 0, r = 0); the calculated values of  $\rho_{f_0}$  remained  $\geq 2 \times$  smaller than the data under all conditions investigated. This is illustrated in Fig. 5 for the  $l_i = 2 \mu m$  case (dotted line).

In summary, we found that comparably good agreement between theory and experiment could be obtained for  $r \approx 0.31$ -0.74 for reasonable values of p and  $\rho l$ . This is due to the fact that the shapes of the theoretically calculated  $\rho_t(d)$  curves for the different combinations of r, p, and  $\rho l$  (Table 2) are not significantly different from one another compared to the scatter in the data. Thus, the relative contributions to  $\rho_{to}(d)$  of surface and grain-boundary scattering cannot be determined very well by applying these theories to our data.

## **Discussion**

There are several factors which suggest that grain-boundary scattering may be the dominant electron-scattering mechanism in  $\mathrm{AuIn_2}$  films. If surface scattering were dominant, the temperature-dependent portion of the  $\mathrm{AuIn_2}$  film resistivity at 300 K,  $\rho_\mathrm{T}=(\beta-1)\rho_\mathrm{fo}$ , would be smaller than the bulk resistivity [3, 10]. The value of  $\rho_\mathrm{T}$  previously observed for 280-nm-thick  $\mathrm{AuIn_2}$  films [3] and those values observed for the  $\mathrm{AuIn_2}$  films in our investigation are found to be comparable to the bulk value of  $\approx 7.5~\mu\Omega\text{-cm}$  [7], indicating that surface scattering is not the main factor that determines  $\rho_\mathrm{fo}$ .

The available  $\rho l$  data for metals suggest that  $\rho l$  for AuIn<sub>2</sub> is likely to be closer to  $0.8 \times 10^{-11} \,\Omega$ -cm<sup>2</sup> than to  $3 \times 10^{-11} \,\Omega$ -cm<sup>2</sup>. Of the approximately twenty metals for which we have  $\rho l$  data, only Cs and K have  $\rho l$  values that exceed  $2.2 \times 10^{-11} \,\Omega$ -cm<sup>2</sup>. Values of 0.7- $1.5 \times 10^{-11} \,\Omega$ -cm<sup>2</sup> are most common. In and Au have values of  $1.5 \times 10^{-11} \,\Omega$ -cm<sup>2</sup> and  $0.92 \times 10^{-11} \,\Omega$ -cm<sup>2</sup>, respectively. From Fig. 5 it is evident that the contributions to  $\rho_t$  of surface scattering

(dotted curve) and grain-boundary scattering (the difference between the solid and dotted curves) are comparable for  $\rho l \approx 3 \times 10^{-11}~\Omega\text{-cm}^2$ , even assuming maximum surface scattering. Thus, for  $\rho l < 3 \times 10^{-11}~\Omega\text{-cm}^2$ , as is likely for our AuIn<sub>2</sub> films, grain-boundary scattering would be dominant.

Thus, the evidence suggests that grain-boundary scattering may be more important in AuIn, films than in other pure metal films. Why this would be the case is not clear. Although incorporation of impurities from the residual gas background present during film deposition has been reported to cause such increased grain-boundary scattering in Mo films [15], this effect does not seem to be important in our work. When the deposition rates of Au and In were increased by  $\approx 5 \times$  to reduce the concentration of gaseous impurities, the  $\rho_{fo}$  values for AuIn<sub>2</sub> films increased ≈20% for Au and remained essentially unchanged for In. This result is probably due to decreasing grain size with increasing deposition rate, and is contrary to what would be expected if incorporation of gaseous impurities were important. Another possibility is that the more complex grain-boundary structure expected for intermetallic compound films results in greater electron scattering than is observed for pure metals.

#### Summary

The influences of film thickness and composition on the resistivity and microstructure of AuIn, films have been investigated. The resistivity at 4.2 K was found to be pprox5  $\mu\Omega$ -cm for 40-nm-thick films and to vary as  $ho_{_{\mathrm{fo}}} \propto d^{-0.76}$ over the thickness range 30-250 nm. Resistivity changes were also observed as the composition was altered. A decrease of ≈10% in the In/Au thickness ratio from that of AuIn<sub>2</sub> produced an increase of  $\approx 50\%$  in  $\rho_{to}$ . A similar increase in In/Au ratio produced a ≤10% decrease in resistivity. Electron microscopic analysis revealed that the grain size of AuIn, films increases with film thickness, and is  $\approx 2 \times$  smaller for the films with In/Au <3.074 than for those ≥3.074. Small regions of darker contrast ("particles") were also observed on or within all films having compositions near that of AuIn, however, their effect on the film resistivity was judged to be negligible.

The factors governing the resistivity of  $\operatorname{AuIn}_2$  films have been analyzed using Fuchs surface-scattering and Mayadas-Shatzkes grain-boundary-scattering theories. It is found that M-S theory can be used to explain the  $\rho_{fo}$  data for a range of r and p values. Reasonable agreement was obtained for parameter values between  $r=0.31, p=0, \rho l=3\times 10^{-11}\,\Omega\text{-cm}^2$  and  $r=0.74, p=1, \rho l=0.8\times 10^{-11}\,\Omega\text{-cm}^2$ . The available evidence is interpreted as favoring grain-boundary scattering as the dominant scattering mechanism.

## **Acknowledgments**

This work is based on the process developed by S. K. Lahiri. The original work relating resistivity to grain-size variations using SEM was completed by him in 1974.

The authors thank C. Serrano for carrying out the TEM work and R. Drake, V. Tom, and A. Ginzberg for assistance with sample preparations and measurements. Helpful discussions with colleagues J. Janak, A. F. Mayadas, and M. Murakami are gratefully acknowledged.

#### References

- J. H. Greiner, S. Basavaiah, and I. Ames, J. Vac. Sci. Technol. 11, 81 (1974); J. H. Greiner et al., IBM J. Res. Develop. 24 (1980, this issue).
- L. M. Geppert, J. H. Greiner, D. J. Herrell, and S. Klepner, IEEE Trans. Magnetics MAG-15, 412 (1979).
- 3. S. K. Lahiri, Thin Solid Films 41, 209 (1977)
- 4. D. J. Herrell, IEEE J. Solid-State Circuits SC-10, 360 (1975).
- A. J. Warnecke, R. M. Patt, and C. J. Johnson, Jr., Kodak Microelectronics Seminar Proceedings (INTERFACE '77), Eastman Kodak Company, Rochester, NY, 1978, p. 145.
- (a) F. A. Shunk, Constitution of Binary Alloys, Second Supplement, McGraw-Hill Book Co., Inc., New York, 1969, p. 72; (b) J. W. Matthews, C. J. Kircher, and R. E. Drake, Thin Solid Films 47, 95 (1977).

- 7. J. P. Jan and W. B. Pearson, Phil. Mag. 8, 279 (1963).
- E. S. Kirkpatrick and A. F. Mayadas, J. Appl. Phys. 44, 4370 (1973).
- 9. E. H. Sondheimer, Adv. Phys. 1, 1 (1952).
- K. L. Choppra, Thin Film Phenomena, McGraw-Hill Book Co., Inc., New York, 1969.
- A. F. Mayadas and M. Shatzkes, Phys. Rev. B 1, 1382 (1970).
- 12. C. R. Tellier, Electrocomponent Sci. Technol. 5, 127 (1978).
- 13. J. M. Ziman, *Principles of the Theory of Solids*, Cambridge University Press, Cambridge, England, 1964.
- N. F. Mott and H. Jones, Theory of the Properties of Metals and Alloys, Oxford University Press, London, England, 1936.
- 15. Hideo Oikawa, J. Vac. Sci. Technol. 15, 1117 (1978).

Received April 20, 1979; revised November 1, 1979

The authors are located at the IBM Thomas J. Watson Research Center, Yorktown Heights, New York 10598. The authors' names are given in alphabetical order.